Catalysis Today xxx (xxxx) xxx–xxx

Contents lists available at ScienceDirect

Catalysis Today

journal homepage: www.elsevier.com/locate/cattod

Catalytic Teflon AF-2400 membrane reactor with adsorbed *ex situ* synthesized Pd-based nanoparticles for nitrobenzene hydrogenation

Baldassarre Venezia[a], Luca Panariello[a], Daniel Biri[a], Juhun Shin[b], Spyridon Damilos[a], Anand N.P. Radhakrishnan[a], Chris Blackman[b], Asterios Gavriilidis[a,*]

[a] Department of Chemical Engineering, University College London, Torrington Place, London, WC1E 7JE, UK
[b] Department of Chemistry, University College London, 20 Gordon Street, London, WC1H 0AJ, UK

ARTICLE INFO

Keywords:
Layer-by-layer assembly
Polydopamine
Tubular membrane
Flow reactor
Colloidal nanoparticles
Palladium catalyst

ABSTRACT

Among the unconventional approaches of supporting catalyst nanoparticles, the layer-by-layer assembly of polyelectrolyte multilayers for nanoparticle adsorption represents an easy and convenient method. It enables the deposition of singularly adsorbed nanoparticles and prevents them from aggregating. In this work, polydopamine was grafted onto the internal surface of a Teflon AF-2400 tubular membrane, known for its excellent permeability to light gases and inertness to chemicals. Poly(acrylic acid) and poly(allylamine hydrochloride) were sequentially adsorbed onto the modified surface of the membrane. *Ex situ* synthesized spherical, cubical, truncated octahedral palladium or dendritic platinum-palladium nanoparticles were then incorporated. The catalytic membranes were assembled in a tube-in-tube configuration and tested over 6 h of continuous nitrobenzene hydrogenation with molecular hydrogen. Stable conversion was observed for the truncated octahedral and dendritic nanoparticles, while a progressive deactivation occurred for the other nanoparticles. Due to their small size, the 3.7 nm spherical nanoparticles exhibited the highest reaction rate, 629$mol_{reactant}$/($mol_{catalyst}$·h), while the cubical nanoparticles showed the highest turnover frequency, ~3000 h^{-1}. The reactor concept developed in this work demonstrates how such a design can serve as a platform for conducting continuous multiphase catalytic reactions in flow using singularly adsorbed and finely tuned nanoparticles. The small volume of pressurized gas present in the tube-in-tube reactor offers improved process safety compared to a batch process, while the Teflon AF-2400 membrane provides control over the gas permeation during reaction.

1. Introduction

Nanocatalysis has attracted considerable attention over recent years [1–3]. The large surface-to-volume ratio of catalyst nanoparticles offers a higher catalyst activity with respect to their bulk equivalent [4–6]. In addition to a size effect, nanoparticle morphology can be of interest in catalysis, due to the different reactivity of crystalline facets [2,6–8]. However, because of their thermodynamic tendency to aggregate, it is of paramount importance to stabilize them onto supports, inorganic or organic [9,10]. Inorganic porous supports for catalytic nanoparticles have been extensively used [10–12], including carbon [13], silica/mesoporous silica [14–16], or zeolites [17].

However, the synthesis of these supports generally includes a high temperature calcination process of the inorganic precursors [18]. Recent trends in supporting nanoparticles on polymeric structures have attracted attention due to the low temperature and environmental friendliness of the preparation process [19]. The layer-by-layer (LbL) polyelectrolyte assembly has been proven to be a versatile method to create nanocomposite structures [20]. This approach consists of alternating polyelectrolyte layers that interact electrostatically *via* their functional building blocks, creating ultrathin organic films [21]. Decher in 1991 developed the concept of the consecutive adsorption of polyelectrolytes, after reporting a method on the successive physisorption of anionic and cationic bipolar amphiphiles onto charged surfaces [22,23]. The layer-by-layer assembly method of polyelectrolytes has been employed in different fields, for both fundamental and applied research, and among these is the adsorption of nanoparticles [20]. In this regard, the work by Dotzauer *et al.* showed that the LbL method can be applied to porous membranes in order to adsorb nanoparticles for catalytic applications [24,25]. The internal surfaces of alumina and polycarbonate membranes were modified by the adsorption of poly (acrylic acid) (PAA) and poly(allylamine hydrochloride) (PAH), which provided binding sites for gold nanoparticles [24]. These were employed in the hydrogenation of 4-nitrophenol into 4-aminophenol by

* Corresponding author.
E-mail address: a.gavriilidis@ucl.ac.uk (A. Gavriilidis).

https://doi.org/10.1016/j.cattod.2020.03.062
Received 7 December 2019; Received in revised form 8 March 2020; Accepted 27 March 2020

sodium borohydride, which flowed through the membrane pores. Results showed that the LbL method was effective in creating catalytic sites inside the membrane and allowing for continuous operation.

Liu *et al.* applied the LbL method to deposit polyelectrolyte layers onto the outer surface of a polypropylene hollow fibre membrane. Catalyst particles were then immobilized onto the modified surface by reducing the adsorbed precursor species [26]. Nitrobenzene hydrogenation to aniline was studied by pumping it outside the tubular membrane, while hydrogen was pressurized inside, in a membrane reactor configuration. The reactor showed stable conversion over hours and process conditions were varied to prove the flexibility of this catalytic membrane reactor. However, the synthesis of nanoparticles performed *in situ*, showed a consequent loss of control over the catalytic particle size and morphology. *Ex situ* synthesis can provide better tuning of the nanoparticles [27,28]. The adsorption of *ex situ* 12 nm Au nanoparticles inside LbL-modified polyethersulfone hollow fibre membranes was demonstrated by Ouyang *et al.* [29]. This study showed that the fibre surface modification led to a high density of unaggregated nanoparticles that were highly active in the continuous liquid phase hydrogenation of 4-nitrophenol.

Dense, hydrophobic, gas-permeable membranes that show high liquid pressure breakthrough, like the Teflon AF-2400, have recently attracted considerable interest, due to their high permeability to light gases and chemical inertness [30,31]. Teflon AF-2400 has been employed in a variety of gas-liquid and gas-liquid-solid reactions [32–37]. First introduced by the group of Ley [38], Teflon AF-2400 has been employed in a tube-in-tube configuration for both homogeneous and heterogeneous continuous hydrogenations. Hydrogen was pressurized outside, while the reacting liquid was directed inside the membrane [33]. In the case of homogeneous catalysis, the catalyst was premixed with the substrate and flowed in the tubular reactor, while when a heterogeneous catalyst was employed, the catalyst was packed in a column placed downstream of the tube-in-tube, which was used as pre-saturator.

In order to be able to support the catalyst on the surface of a tubular Teflon AF-2400 membrane using an LbL approach, an initial surface modification is required. The discovery in 2007 of the adhesive properties of polydopamine (PDA) onto different materials by the group of Messersmith [39], paved the way for applications of PDA coatings in material science, chemistry and engineering [40]. PDA contains aminoethyl and catechol functional groups, which respectively display a positive and negative charge, making it suitable in the LbL assembly method [41].

In this work, the inner surface of a tubular Teflon AF-2400 membrane was modified, *via* a PDA coating followed by the sequential deposition of a PAA and PAH layers. Nitrobenzene hydrogenation with molecular hydrogen was used as a model reaction and was carried out over size- and shape-tuned *ex situ* synthesized palladium-based nanoparticles that were adsorbed onto the inner surface of the modified tubular membrane. Palladium was chosen as the catalyst due to its high selectivity in the hydrogenation of the nitro group [42]. Characterization analyses and reaction tests were performed on different adsorbed nanoparticles, demonstrating this reactor concept as an attractive platform for nanoparticle catalyst testing.

2. Materials and methods

2.1. Nanoparticle synthesis

Sodium tetrachloropalladate(II) (Na_2PdCl_4, 99.99 %), potassium tetrachloroplatinate(II) (K_2PtCl_4, 99.99 %), polyvinylpyrrolidone (PVP, Mn ~55,000), potassium bromide (FT-IR grade, ≥99 %), L-ascorbic acid (reagent grade), citric acid monohydrate (ACS reagent, ≥99.0 %) and Pluronic® P123 (PEG-PPG-PEG, Mn ~5,800) were purchased from Sigma Aldrich.

2.1.1. Pd nanospheres synthesis

Pd nanospheres were synthesized according to Piao *et al.* [43]. In detail, 29.4 mg of Na_2PdCl_4 were dissolved in 1 mL of deionized (DI) water. Separately, 200 mg of PEG-PPG-PEG were dissolved in 10 mL of DI water. After the complete dissolution of the polymer, 0.1 mL of the Pd precursor solution were injected in the polymer solution and stirred for 24 h at room temperature.

2.1.2. Pd truncated nano-octahedra synthesis

Pd nano-octahedra were prepared according to Lim *et al.* [44]. In detail, 68.4 mg of Na_2PdCl_4 were dissolved in 3.6 mL of DI water. Separately, 105 mg of PVP, 60 mg L-ascorbic acid and 60 mg of citric acid were dissolved in 8 mL of DI water and heated to 100 °C under reflux in a stirred three-neck flask placed in an oil bath. A volume of 3 mL of the Pd precursor was then injected in the heated flask. After 3 h, the solution was removed from the oil bath and allowed to cool at room temperature in open air.

2.1.3. Pd nanocubes synthesis

Pd nanocubes were prepared according to Lim *et al.* [45]. In detail, 67.1 mg of Na_2PdCl_4 were dissolved in 3.6 mL of a 1.68 M KBr water solution the day before the synthesis. On the day of the synthesis, 105 mg of PVP, 60 mg L-ascorbic acid and 60 mg of citric acid were dissolved in 8 mL of DI water and heated to 80 °C in a stirred three-neck flask placed in an oil bath. Then, 3 mL of the prepared Pd precursor stock were injected in the heated solution. After 3 h, the solution was removed from the bath and allowed to cool at room temperature in open air.

2.1.4. Pt-Pd nanodendrites synthesis

Pt-Pd nanodendrites were prepared according to Lim *et al.* [44]. In detail, Pd nano-octahedra were prepared as previously described. Then, 1 mL of this solution was added to 6 mL of DI water. In this solution, 35 mg of PVP and 60 mg L-ascorbic acid were dissolved. This solution was heated to 90 °C in a stirred three-neck flask placed in an oil bath. Separately, 27 mg of K_2PtCl_4 were dissolved in 3 mL of DI water. This solution was then injected in the heated solution containing the Pd nano-octahedra, PVP and ascorbic acid. After 3 h, the solution was removed from the heating bath and allowed to cool at room temperature in open air.

After the synthesis, each colloidal solution was transferred into a dialysis membrane (Mw cut-off: 12 – 14 kDa, Medicell Membranes Ltd) placed in a DI water bath for 24 h. This was performed in order to remove unreacted precursors and excess of reducing agent.

2.2. Membrane modification and nanoparticle adsorption

The tubular Teflon AF-2400 membrane (internal diameter, ID: 0.8 mm, outer diameter, OD: 1.0 mm, length: 30 cm, Biogeneral) was functionalized with PDA. The polymerization of dopamine was performed in a basic environment and triggered by oxygen dissolved in the solution. The procedure was taken from Messersmith and co-workers [39,40]. All polymeric solutions were pumped using plastic syringes (20 mL, HSW) and a syringe pump (PHD ULTRA, Harvard Apparatus). Polydopamine was prepared mixing 16 mg dopamine hydrochloride (Sigma Aldrich) and dissolving it in a 8 mL buffer solution at a pH of 8.5 (Tris-HCl 0.010 M, 2BScientific). The solution was pumped at 17 μL/min through the membrane for 8 h. Afterwards, the buffer solution was pumped for 1 h at a flowrate of 20 μL/min. The membrane was then dried in an oven (Lenton) at 60 °C overnight. The procedure for the adsorption of the following polyelectrolytes was similar to the one adopted by Dotzauer *et al.* and Liu *et al.* [24,46]. The anionic polyelectrolyte solution was prepared by mixing 0.67 mL of poly(acrylic acid) (PAA, Mw ~5,000, Sigma Aldrich) with 3.33 mL of DI water and 117 mg of NaCl. The pH was increased by dropwise addition of 2 M NaOH (Sigma Aldrich) until a pH value of 3 was reached. The polyelectrolyte solution was then pumped at a flowrate of 20 μL/min for 2 h through the PDA-modified membrane. Afterwards, DI water was pumped at 40 μL/min for 1 h and subsequently the membrane was

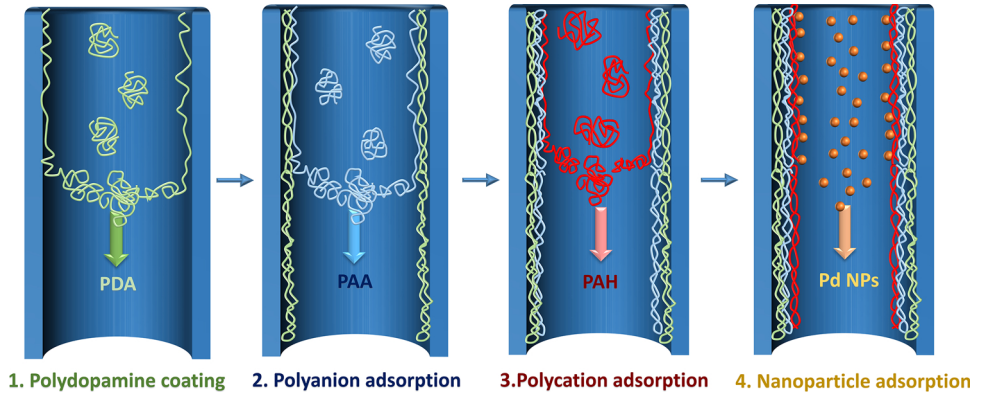

Fig. 1. Graphical representation of the PDA/PAA/PAH layer-by-layer modification of a Teflon AF-2400 tubular membrane followed by adsorption of palladium nanoparticles (PDA: polydopamine, PAA: poly(acrylic acid), PAH: poly(allylamine hydrochloride)).

placed in the oven at 60 °C for 2 h. The preparation of the cationic polyelectrolyte was performed by dissolving 700 mg of poly(allylamine hydrochloride) (PAH, Mw ~17,500, Sigma Aldrich) in 2 mL DI water and 58 mg NaCl. The mixture was stirred until a clear and homogeneous solution was obtained. The pH was raised to 6.5 by gradual dropwise addition of 2 M NaOH. The final polymeric mixture was pumped at a flowrate of 20 µL/min through the membrane for 2 h. DI water was then pumped at 40 µL/min for 2 h, followed by drying in the oven at 60 °C for 2 h. Nanoparticle adsorption was carried out by pumping the nanoparticle solution at 10 µL/min through the LbL-modified Teflon AF-2400 tubular membrane for 12 h. Fig. 1 is a graphical representation of the steps for making the Teflon AF-2400 membrane catalytic, involving an LbL-modification of the internal surface followed by nanoparticle adsorption.

2.3. Materials characterization

Prior to adsorption, the nanoparticles were characterized by transmission electron microscopy (TEM, 2100 EXii, 120 kV acceleration voltage, JEOL) in order to determine their average size and morphology. Surface characterization analyses were performed before reaction. Pieces from the membranes were cut along the axial dimension and flattened. Atomic force microscopy (AFM, Dimension Icon, Bruker) was used for the visualization of the Teflon AF-2400 membrane before and after the LbL modification, and after nanoparticle deposition. The AFM was used in Peak Force Tapping Mode at 2 kHz Peak Force Frequency and 0.5–1 Hz line rate at 256 scans per line resolution. Post-processing of the raw pictures was performed by a second degree polynomial flattening. X-ray photoelectron spectroscopy (XPS, K-alpha, Al source 1486.6 eV, Thermo Scientific) was employed in order to detect the surface elemental composition and the palladium oxidation state on the modified membrane. The XPS data were calibrated to an ionization attributed to adventitious carbon at 285.0 eV. To determine the metal loading of the catalytic membranes before and after reaction, inductively coupled plasma mass spectroscopy (ICP-MS, 820, Varian) was used. For this characterization, the membranes were cut into pieces and aqua regia (3 volumes HCl, 1 volume HNO_3) was used to dissolve the metal nanoparticles to obtain a leachate, which was used for analysis.

2.4. Nitrobenzene hydrogenation

Nitrobenzene hydrogenation was employed as model reaction to perform a comparative study of the catalytic performance of the palladium-based nanoparticles. Scheme 1 shows the generally accepted reaction mechanism [47,48]. There are two relevant reaction pathways. The first is the direct three-step reduction of the nitro group into the nitroso, hydroxylamine and amine group. The second pathway involves a condensation reaction of nitrosobenzene and N-phenylhydroxylamine to produce azoxybenzene, which can be further reduced into aniline in a three-step hydrogenation involving the consecutive production of azobenzene and hydrazobenzene. However, the mechanism for nitrobenzene hydrogenation still represents a topic of research and a clear reaction mechanism has not been established yet [47,49].

2.5. Reactor design and operation

The LbL-modified catalytic membranes were cut to a length of 20 cm, with an inner surface area of 5 cm^2 covered with nanoparticles. They were assembled inside a 15 cm long polytetrafluoroethylene

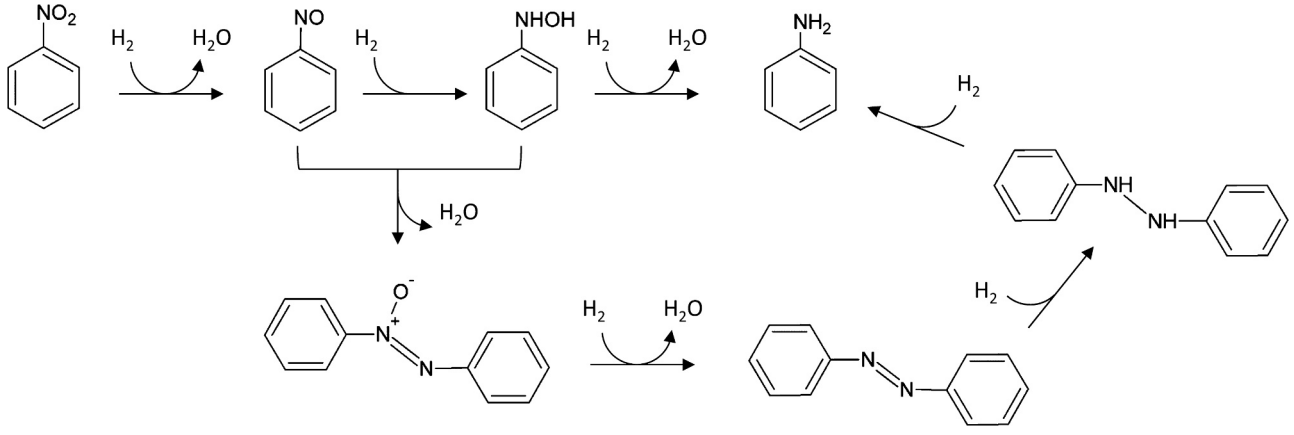

Scheme 1. Reaction pathways for the reduction of nitrobenzene to aniline.

(PTFE) tube (ID: 0.063″, OD: 1/8”, Thames Restek), in a tube-in-tube configuration, using two polyether ether ketone (PEEK) T-junctions (Upchurch) that sealed the membrane to the inlet and outlet tubes. Pure hydrogen from a hydrogen generator (PH200, Peak Scientific) was pressurized in a dead-end configuration outside the membrane (the gas outlet T-junction was sealed). Hydrogen was delivered from the other T-junction, permeated through the membrane and reacted on the palladium-based nanoparticles with nitrobenzene which flowed inside the membrane. A solution of nitrobenzene in the concentration range of 30 − 100 mM in ethanol (both Sigma Aldrich) was placed inside an 8 mL stainless-steel syringe (Harvard Apparatus) and was pumped by means of a syringe pump (PHD ULTRA, Harvard Apparatus) at a constant flowrate of 15 μL/min. This corresponded to a residence time of ~5 min inside the reactor. The syringe was connected to the inlet of the tube-in-tube reactor, while the outlet was connected to a pressure sensor (P X 309, Omega) and to an adjustable back-pressure regulator (BPR-01, Zaiput). These were used to keep the liquid pressure inside the membrane at 6 bar, while the hydrogen was stagnant and pressurized at 5 bar outside the membrane. The lower gas pressure was used to prevent the formation of bubbles into the liquid. Fig. 2 shows the schematic of the set-up. The tube-in-tube reactor was kept inside a bath filled with water and placed on a hotplate (US152, Stuart). A constant and uniform water temperature of 30 °C was maintained and measured by a thermocouple immersed inside the bath and connected to the hotplate.

Samples were analyzed by a gas chromatograph (7820A, Agilent Technologies) using a flame ionization detector (FID), a HP-INNOWAX (19091 − 133) capillary column and a liquid auto-sampler. The two main products detected were aniline and nitrosobenzene. Taking into account the nitrobenzene, aniline and nitrosobenzene species at the outlet, the nitrogen balance was calculated relative to the concentration of nitrobenzene at the inlet. This value ranged between 98 % and 102 % for all the experiments. Nitrobenzene conversion, X, was calculated using Eq. (1), where $C_{NB,in}$ and $C_{NB,out}$ are the concentration of nitrobenzene at the inlet and the outlet of the reactor. Eqs. (2) and (3) define product selectivity for aniline, S_{AN}, and nitrosobenzene, S_{NS}, respectively. Here $C_{AN,out}$ and $C_{NS,out}$ are the concentrations of aniline and nitrosobenzene at the outlet of the reactor.

$$X = \frac{C_{NB,in} - C_{NB,out}}{C_{NB,in}} \tag{1}$$

$$S_{AN} = \frac{C_{AN,out}}{C_{NB,in} - C_{NB,out}} \tag{2}$$

$$S_{NS} = \frac{C_{NS,out}}{C_{NB,in} - C_{NB,out}} \tag{3}$$

The average nitrobenzene consumption rate, r, was calculated according to Eq. (4), where $F_{NB,in}$ is the inlet molar flowrate of nitrobenzene and n_{metal} the molar amount of palladium metal in the reactor. For the Pt-Pd nanodendrites the total amount of palladium and platinum metal was taken into account, despite the latter being much higher than the former. To estimate the activity of surface atoms, a turnover frequency, TOF, was defined according to Eq. (5), where R is the ratio between the number of bulk atoms below the first external atomic layer to the total amount of metal atoms in the nanoparticle. Hence, 1-R is the nanoparticle dispersion and its estimation is reported in the Supplementary Information.

$$r = \frac{X\, F_{NB,in}}{n_{metal}} \tag{4}$$

$$TOF = \frac{r}{1 - R} \tag{5}$$

3. Results and discussion

3.1. TEM characterization of nanoparticles

Nanoparticle size and morphology were analyzed *via* TEM and size distribution was obtained using Pebbles [50]. At least 120 particles per

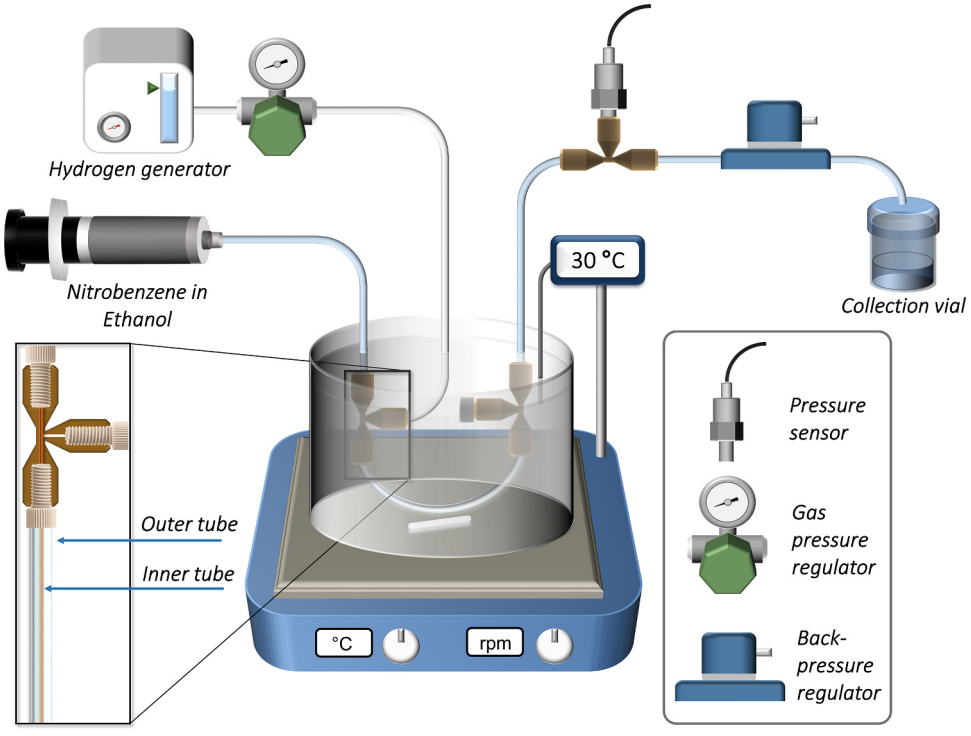

Fig. 2. Experimental set-up schematic of the tube-in-tube LbL-modified Teflon AF-2400 membrane reactor for the continuous hydrogenation of nitrobenzene on palladium-based nanoparticles.

Table 1
Average particle size along with standard deviation of palladium-based nanoparticles, obtained by TEM.

Nanoparticle	Average particle size, nm
Pd nanospheres	3.7 ± 0.6
Pd truncated nano-octahedra	3.9 ± 0.6
Pd nanocubes	24.9 ± 3.7
Pt-Pd nanodendrites	6.2 ± 1.2

sample were analyzed. Average nanoparticle sizes are presented in Table 1 along with their standard deviation, while TEM pictures are reported in the Supplementary Information.

3.2. Atomic force microscopy analysis of membranes

Atomic force microscopy micrographs of the membrane surface before adsorption of the nanoparticles are presented in Fig. 3. The pristine Teflon membrane surface presents a relatively smooth surface with an elevation difference of around 10 nm between the lowest and the highest point. Fig. 3 also displays the modified surface of the membrane after the LbL sequential adsorption of the polyelectrolyte multilayers. It is evident that the surface lost its smoothness after the modification, presenting bulges with an average size of 100 nm and elevation of *ca.* 25 nm. Fig. 4 shows the micrographs of the inner surface of the membrane with the adsorbed palladium-based nanoparticles. The surface covered with spherical nanoparticles presented scattered bulges, which can be ascribed to the polyelectrolyte assembly, features with a characteristic size in the order of 10 nm and singularly resolved nanoparticles. The surface covered with truncated octahedral nanoparticles displayed homogeneously adsorbed singular nanoparticles. It is possible to observe that some bulges created during the LbL modification provided higher adsorption surface and are covered by the nanoparticles. For the case of the dendritic Pt-Pd nanoparticles, these could be observed in the form of clusters of nanoparticles with dimensions larger than 40 nm. The cubes, which were approx. 25 nm were singularly resolved by AFM analysis. They were scattered over a wavy surface and some of them were found buried inside the polymeric support.

3.3. X-ray photoelectron spectroscopy analysis of membranes

XPS revealed palladium and platinum on the inner surface of the catalytic membranes (see Supplementary Information). Fig. 5 shows the high resolution Pd 3d overlay spectra of all samples. Despite the low signal-to-noise ratio, it is possible to observe that the peaks of the spherical, truncated octahedral and dendritic nanoparticles are shifted to approx. 0.3 eV higher energy as compared to the cubical nanoparticles. The main Pd $3d_{5/2}$ peak observed for the cubical nanoparticles was at 335.0 eV, attributed to metallic palladium. This suggests that the Pd cubical nanoparticles displayed less oxidation compared to the Pd spherical, truncated octahedral and dendritic nanoparticles.

3.4. Hydrogenation of nitrobenzene in flow

3.4.1. Effect of substrate concentration

Continuous reaction experiments with the LbL-modified catalytic tubular membrane were performed over more than 6 h. The effect of two nitrobenzene concentrations, namely 30 mM and 100 mM, was studied using palladium nanospheres. Conversion and product selectivities are reported in Fig. 6. Nitrobenzene conversion for the lower concentration reached completion over the whole reaction period, along with a selectivity to aniline in the range of 95–100 %. Conversely, for the case of 100 mM, conversion dropped from 36 % to 26 % after 6 h of operation. Selectivity to aniline ranged between 85–88 % and nitrosobenzene selectivity increased to 15 % in the last hours of reaction. This difference can be ascribed to the fact that at a higher concentration of nitrobenzene, the nitrosobenzene produced in the first reaction step could not be further hydrogenated under the same catalyst contact time. However, at a lower substrate concentration the nitrosobenzene produced could be fully hydrogenated into aniline. Moreover, using around 3-fold higher substrate concentration, conversion dropped by *ca.* a factor of three, from 95 to 100 % to 30–40 %. The maximum possible hydrogen supply rate through the membrane was estimated to be 2.9 mL/min, assuming full consumption of hydrogen at the catalyst location (see Supplementary Information). On the other hand, considering a conversion of 100 % of nitrobenzene to aniline at a flowrate of 15 µL/min and an inlet concentration of 100 mM, the hydrogen consumption rate was assessed to be only 0.1 mL/min. It is therefore reasonable to assume that there was no limitation of hydrogen supply.

3.4.2. Comparison of catalytic performance of different types of nanoparticles

Reaction experiments involving the use of palladium-based nanoparticles with different morphology and size were carried out over a period of 6 − 7 h of continuous reaction. The nitrobenzene inlet concentration was kept constant at 100 mM, along with a temperature of 30 °C and hydrogen pressure of 5 bar and results are presented in Fig. 7.

As seen in Fig. 7, the nanocubes showed 96 % conversion in the first hour of operation, but this value steadily dropped to 54 % after 6.5 h. Over the whole reaction period, selectivity to nitrosobenzene increased from 5 % to 12 % while aniline selectivity dropped from 95 % to 88 %, possibly because of the simultaneous drop in conversion. The palladium truncated nano-octahedra exhibited much lower but steady conversion (7–8 %) after 2 h reaction time and higher selectivity to nitrosobenzene,

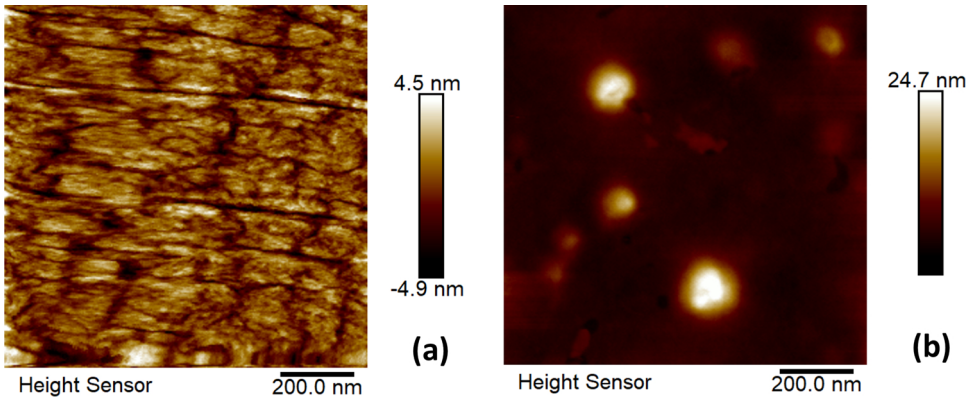

Fig. 3. AFM micrographs of (a) pristine Teflon AF-2400 membrane and (b) LbL-modified PDA/PAA/PAH membrane inner surface before adsorption of nanoparticles.

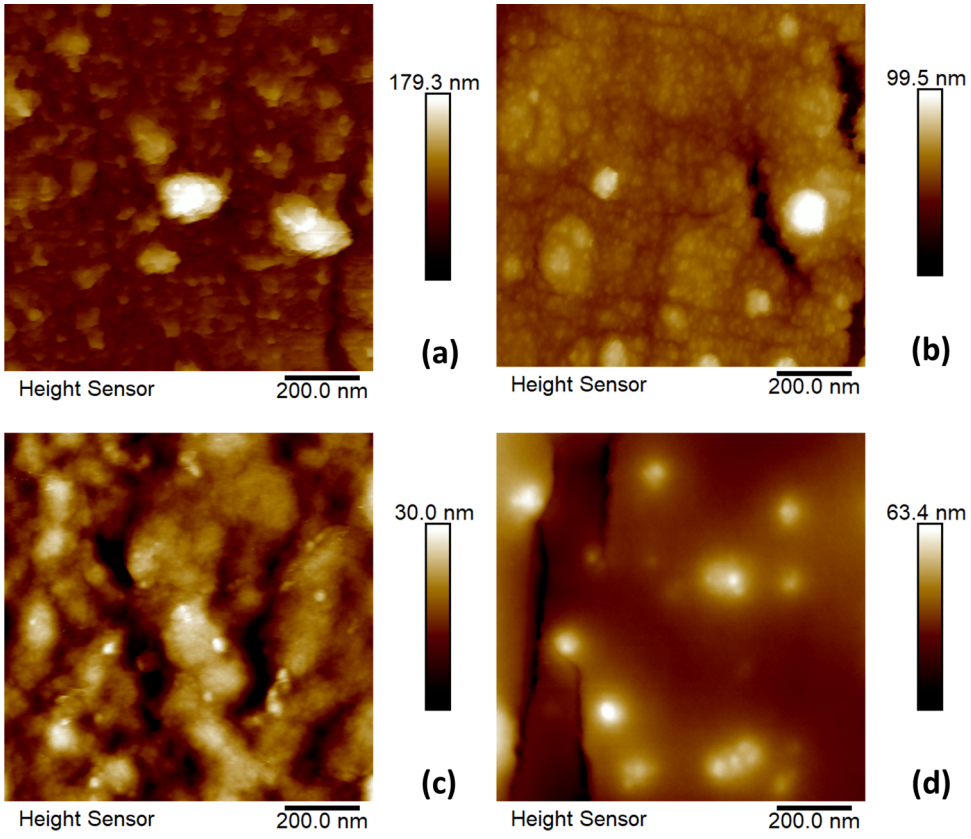

Fig. 4. AFM micrographs of the LbL-modified PDA/PAA/PAH tubular Teflon AF-2400 membrane inner surface after the adsorption of (a) Pd spherical, (b) Pd truncated octahedral, (c) Pd cubical and (d) Pt-Pd dendritic nanoparticles.

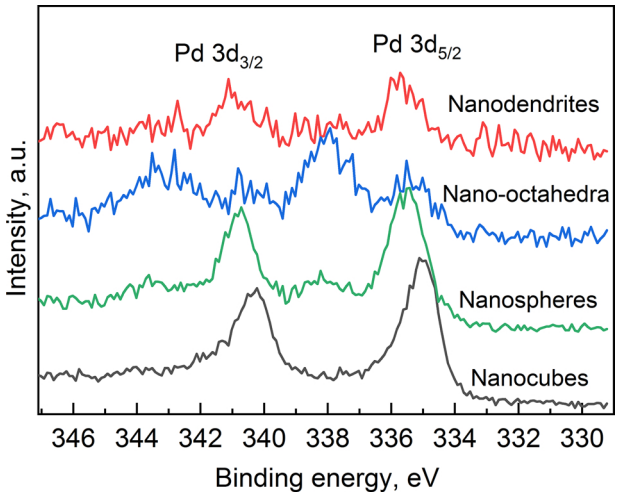

Fig. 5. X-ray photoelectron spectra of the Pd 3d region of the spherical, truncated octahedral, cubical and dendritic nanoparticles adsorbed over the LbL-modified PDA/PAA/PAH Teflon AF-2400 tubular membrane inner surface.

with an aniline selectivity of 75 %. An even lower selectivity to aniline, at higher conversion values, was recorded for the platinum-palladium nanodendrites. Despite a first drop from 35 % to 21 % in the first 2 h of operation, conversion was stable for more than 4 h, with a selectivity to nitrosobenzene and aniline equal to 40 % and 60 % respectively. In the work of Kataoka *et al.* a similar selectivity of 40 % to nitrosobenzene was achieved using platinum nanoparticles immobilized inside a catalyst-coated capillary microreactor [48]. An inlet concentration of 50 mM nitrobenzene at a flowrate of 10 μL/min was employed along with 100 μL/min hydrogen flowrate.

ICP-MS analysis revealed a palladium and platinum metal content adsorbed in the modified tubular membranes in the range of $0.5-12\,\mu g/cm^2$. These values were determined both before and after the reaction and were used to estimate the consumption rate and the turnover frequency of nitrobenzene reacting on the catalytic nanoparticles. Table 2 shows the results.

Palladium nanospheres showed a conversion of 36 % in the first hours of reaction, with a loading of $1.09\,\mu g/cm^2$, which resulted in a consumption rate of 629 $mol_{reactant}/(mol_{catalyst}\cdot h)$. However, after reaction the nanospheres-loaded membrane presented leaching of around 12 % of the initial loading and a nitrobenzene conversion decrease of 28 %. These values suggest that deactivation cannot be only explained by a mere leaching effect of the catalyst from the reactor, but to other parallel effects, such as poisoning or particle restructuring. Similarly to the nanospheres, but with half the catalyst loading, the truncated nano-octahedra showed an initial *r*of similar value, 538 $mol_{reactant}/(mol_{catalyst}\cdot h)$. This can be ascribed to their similar average particle size. However, unlike the nanospheres, the truncated nano-octahedra exhibited almost no leaching during reaction and their deactivation should be attributed to other effects.

The reaction rate of the Pt-Pd nanodendrites was assessed taking into account both the platinum and the palladium loading. It decreased from ~340 to ~260 h^{-1}, from the start to the end of the reaction. However, a leaching of 29 % from the original platinum loading of $3.38\,\mu g/cm^2$ was observed. The same relative drop was observed for the palladium loading which decreased from $0.17\,\mu g/cm^2$ to $0.12\,\mu g/cm^2$. This effect might be among the possible causes for the drop in conversion from 36 % to 19 % (-47 %). However, based on the external layer of atoms and assuming the nanoparticle as a sphere, the nanodendrites exhibited an initial *TOF* of 1414 h^{-1}, which was of the same order of magnitude as the initial *TOF* of the palladium nanospheres (1628 h^{-1}) and truncated nano-octahedra (1457 h^{-1}).

Results from batch hydrogenations of nitrobenzene using palladium

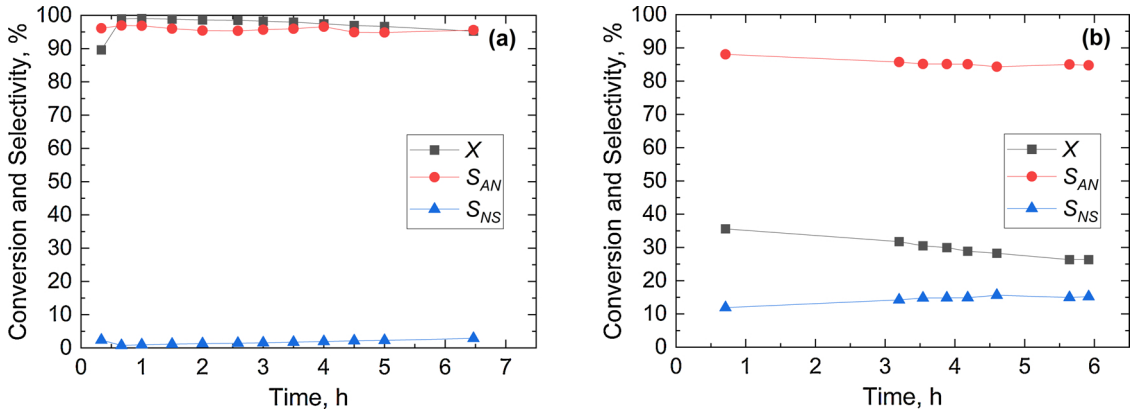

Fig. 6. Nitrobenzene conversion, *X*, aniline selectivity, S_{AN} and nitrosobenzene selectivity, S_{NS}, during the hydrogenation of nitrobenzene in the membrane reactor with the Pd nanospheres. Nitrobenzene inlet concentration, (a) 30 mM, (b) 100 mM. Liquid flowrate, 15 μL/min; liquid pressure, 6 bar; hydrogen pressure, 5 bar; temperature, 30 °C.

nanoparticles resulted in reaction rates in the same order of magnitude as our work. In the work of Huang *et al.*, 2.6 nm Pd nanoparticles stabilized inside P123 micelles in water were tested at 45 °C and 30 bar hydrogen pressure [42]. The reaction rate was 245 $mol_{reactant}/(mol_{catalyst} \cdot h)$ after 2 h reaction time. Harraz *et al.* synthesized 4 nm Pd nanoparticles stabilized by polyethylene glycol in ethanol and tested them at room temperature and 1 bar H_2 pressure. A reaction rate of 126 $mol_{reactant}/(mol_{catalyst} \cdot h)$ after 180 min reaction time was observed [51].

To the best of our knowledge, comparative studies on the effect of palladium nanoparticle morphology in the batch or continuous hydrogenation of nitrobenzene are not reported in the literature. However, such a study was performed for 2-methyl-3-butyn-2-ol hydrogenation over unsupported PVP-stabilized Pd nanocrystals [6]. In that work, it was concluded that the activity of nanocubes and nano-octahedra had a similar trend, while nanocuboctahedra had the lowest activity because of the large presence of edge atoms, which disfavoured the 2-methyl-3-butyn-2-ol hydrogenation.

In our work, estimating the turnover frequency based on the surface atoms of the nanoparticle, we found that the cubical nanoparticles demonstrated the highest *TOF*, in the order of 3000 h^{-1}. This was two times higher than the nanospheres and truncated nano-octahedra. However, the reactor with adsorbed nanocubes exhibited a much larger

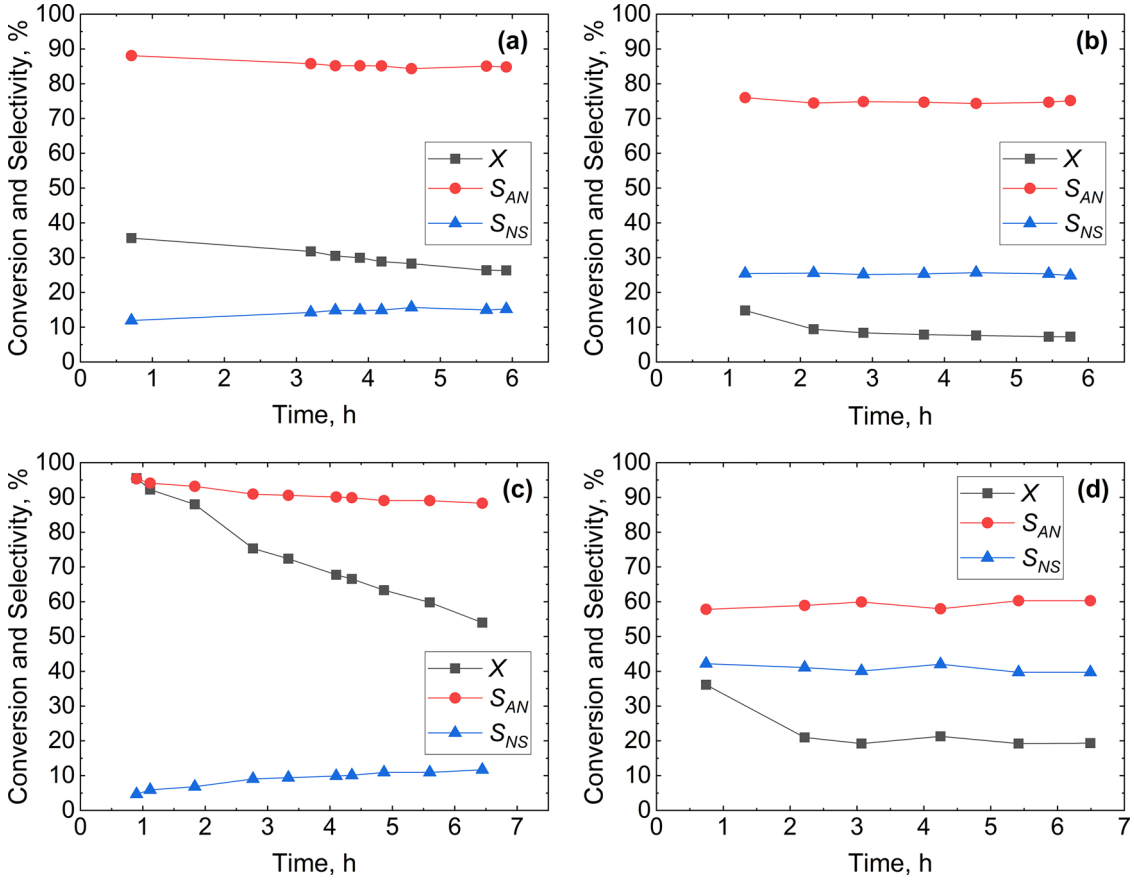

Fig. 7. Nitrobenzene conversion, *X*, aniline selectivity, S_{AN} and nitrosobenzene selectivity, S_{NS}, during the hydrogenation of nitrobenzene in the membrane reactor. The reactor contained (a) Pd nanospheres, (b) Pd truncated nano-octahedra, (c) Pd nanocubes and (d) Pt-Pd nanodendrites. Nitrobenzene inlet concentration, 100 mM; liquid flowrate, 15 μL/min; liquid pressure, 6 bar; hydrogen pressure, 5 bar; temperature, 30 °C.

Table 2
Palladium and platinum metal loading per membrane inner surface, nitrobenzene conversion, *X*, consumption rate, *r*, and turnover frequency, *TOF*, before and after reaction for the Pd spherical, Pd truncated octahedral, Pd cubical and Pt-Pd nanoparticles.

Nanoparticle	Metal loading on the membrane, μg/cm^2		*X*, %		*r*, mol$_{reactant}$/(mol$_{catalyst}$·h)		*TOF*, h^{-1}	
	Start	End	Start	End	Start	End	Start	End
Pd nanospheres	1.09	0.96	36	26	629	515	1628	1332
Pd truncated nano-octahedra	0.56	0.53	15	7	538	239	1457	647
Pd nanocubes	12.18	4.08	96	54	150	252	2293	3854
Pt-Pd nanodendrites (Pt)	3.38	2.37	36	19	341	257	1414	1067
Pt-Pd nanodendrites (Pd)	0.17	0.12	36	19				

conversion drop (−44 %), which can be attributed to Pd leaching of 66 % with respect to the initial loading of 12.18 μg/cm^2. An interesting aspect of the nanocubes adsorption was the 12-fold higher loading that could be achieved compared to the nanospheres, possibly arising from their larger average particle size. The ratio between the average volume of nanocubes (25 nm) and nanospheres (4 nm) can be estimated to be 244. However, the palladium mass ratio between the adsorbed nanocubes and the adsorbed nanospheres was only ~12, which indicates that that a lower number of nanocubes were adsorbed on the membrane surface with respect to nanospheres.

The enhanced *TOF* of the nanocubes can be connected to the XPS results. Their higher reduction degree, as evidenced by their 0.3 eV shift to lower energy, might be the cause for the enhanced activity. Palladium metal has in fact the important role of dissociating and providing surface-reactive hydrogen atoms in the nitrobenzene reaction [52,53]. The higher catalytic activity of the nanocubes can also be related to their larger size compared to the other nanoparticles. Carturan *et al.* showed an increased *TOF* as the degree of metal dispersion decreased, in the batch hydrogenation of nitrobenzene [54]. The authors attributed this to the fact that the larger palladium particles favoured hydrogen dissociation and reduction of the metallic surface, oxidized by the adsorption of nitrobenzene.

Palladium nanoparticles supported on the inner surface of tubular membranes can represent a suitable alternative to packed-bed reactors where internal mass transfer resistances occur inside catalyst particles and the wetting liquid. Experiments with Au-Pd/TiO_2 catalyst packed inside a Teflon AF-2400 tubular membrane were performed in our group and indicated the presence of internal mass transfer resistance [36]. Use of immobilized palladium nanoparticles in flow reactors for the hydrogenation of nitrobenzene can be found in the work of Liu *et al.* [26]. In that work, a polypropylene hollow fibre membrane was modified on its outer surface with PDA followed by poly(sodium 4-styrenesulfonate) and PAH. This was assembled in a tube-in-tube membrane configuration and nitrobenzene hydrogenation was performed in the annulus, while hydrogen was pressurized inside the tubular membrane. The nanoparticles were synthesized *in situ* after adsorption and reduction of the palladium precursor on the external surface of the modified hollow fibre membrane. After 10 h continuous reaction, the catalyst loading was *ca.* 47 μg, and the reactor could achieve a nitrobenzene conversion of 48 %. The inlet substrate concentration was 30 mM with a liquid flowrate of 10 μL/min resulting in an average consumption rate of around 19 mol$_{reactant}$/(mol$_{catalyst}$·h), which was significantly smaller than the one achieved by the nanospheres in our work. This can possibly be due to the much larger average nanoparticle size of 100 nm. In a similar work, using the same inlet nitrobenzene concentration and liquid flowrate, nitrobenzene hydrogenation was performed over a Pd/γ-Al_2O_3 catalyst coated on a poly(dimethylsiloxane) flat membrane with hydrogen flowing on the other side of the membrane [55]. This showed 52 % conversion at 110 mM nitrobenzene inlet concentration, 10 μL/min liquid flowrate and using 1.9 mg catalyst coated on the membrane. The catalytic layer produced in that work was homogeneously distributed over the membrane with a depth of 1 μm.

4. Conclusions

A Teflon AF-2400 tubular membrane was modified *via* adsorption of polyelectrolyte multilayers onto which palladium-based nanoparticles with different size and shapes were adsorbed. The use of a Teflon AF-2400 membrane, allowed operating at high liquid pressure without gas bubble formation in the liquid. AFM showed the presence of adsorbed nanoparticles on the inner surface of the membrane, along with a wavy topography of the membrane surface after modification with the polyelectrolyte assembly. X-ray photoelectron spectroscopy highlighted a shift to high binding energies for the palladium in the spherical, truncated octahedral and dendritic nanoparticles with respect to the cubical. This indicated a higher oxidation state for the these nanoparticles compared to the nanocubes. The catalytic membranes were assembled in a tube-in-tube reactor configuration and tested for nitrobenzene hydrogenation in flow. The palladium nanospheres of 4 nm size showed a stable conversion close to 100 % for over 6 h of continuous reaction with almost no by-product formation, when using 30 mM nitrobenzene inlet concentration; however, deactivation was observed with 100 mM nitrobenzene concentration. A comparative study of the performance of different palladium-based nanoparticles revealed a high consumption rate of nitrobenzene of around 600 mol$_{reactant}$/(mol$_{catalyst}$·h) in the first hours of operation using the Pd nanospheres, attributed to their small size. However, the highest turnover frequency based on the nanoparticle surface atoms was observed for the nanocubes, which was in the order of 3000 h^{-1}. This was possibly due to the lower oxidation state of cubical nanoparticles. Leaching of metals from the reactor was found to be the highest for the one loaded with nanocubes, while almost no losses were recorded in the case of the truncated nano-octahedra.

CRediT authorship contribution statement

Baldassarre Venezia: Conceptualization, Methodology, Writing - original draft, Writing - review & editing, Visualization, Investigation. **Luca Panariello:** Conceptualization, Investigation. **Daniel Biri:** Methodology, Investigation. **Juhun Shin:** Data curation, Investigation. **Spyridon Damilos:** Investigation, Visualization. **Anand N.P. Radhakrishnan:** Data curation, Investigation. **Chris Blackman:** Writing - review & editing, Resources. **Asterios Gavriilidis:** Supervision, Writing - review & editing, Resources.

Declaration of Competing Interest

No competing interests to declare.

Acknowledgements

The authors thank EPSRC for funding (grant EP/L003279/1 and for BV's DTP studentship), Dr Richard Thorogate for the AFM analysis and Prof John McArthur for the ICP-MS analysis.

Appendix A. Supplementary data

Supplementary material related to this article can be found, in the online version, at doi:https://doi.org/10.1016/j.cattod.2020.03.062.

References

[1] D. Astruc, Transition-metal nanoparticles in catalysis: from historical background to the state-of-the art, in: D. Astruc (Ed.), Nanoparticles and Catalysis, 2008, pp. 1–48 Weinheim.
[2] B. Roldan Cuenya, Acc. Chem. Res. 46 (2013) 1682–1691.
[3] F. Zaera, Catal. Lett. 142 (2012) 501–516.
[4] H.-J. Freund, Chem. Eur. J. 16 (2010) 9384–9397.
[5] S. Cheong, J.D. Watt, R.D. Tilley, Nanoscale 2 (2010) 2045–2053.
[6] M. Crespo-Quesada, A. Yarulin, M. Jin, Y. Xia, L. Kiwi-Minsker, J. Am. Chem. Soc. 133 (2011) 12787–12794.
[7] K. An, G.A. Somorjai, ChemCatChem 4 (2012) 1512–1524.
[8] S. Mostafa, F. Behafarid, J.R. Croy, L.K. Ono, L. Li, J.C. Yang, A.I. Frenkel, B.R. Cuenya, J. Am. Chem. Soc. 132 (2010) 15714–15719.
[9] G. Prieto, J. Zečević, H. Friedrich, K.P. de Jong, P.E. de Jongh, Nat. Mater. 12 (2012) 34.
[10] D. Astruc, F. Lu, J.R. Aranzaes, Angew. Chem. Int. Ed. 44 (2005) 7852–7872.
[11] H.-U. Blaser, A. Indolese, A. Schnyder, H. Steiner, M. Studer, J. Mol. Catal. A Chem. 173 (2001) 3–18.
[12] M.L. Toebes, J.A. van Dillen, K.P. de Jong, J. Mol. Catal. A Chem. 173 (2001) 75–98.
[13] A.L. Dantas Ramos, Pd.S. Alves, D.A.G. Aranda, M. Schmal, Appl. Catal. A Gen. 277 (2004) 71–81.
[14] M.K. Richmond, S.L. Scott, H. Alper, J. Am. Chem. Soc. 123 (2001) 10521–10525.
[15] C.P. Mehnert, D.W. Weaver, J.Y. Ying, J. Am. Chem. Soc. 120 (1998) 12289–12296.
[16] C.M. Crudden, M. Sateesh, R. Lewis, J. Am. Chem. Soc. 127 (2005) 10045–10050.
[17] K. Okumura, K. Nota, K. Yoshida, M. Niwa, J. Catal. 231 (2005) 245–253.
[18] H.H. Kung, E.I. Ko, Chem. Eng. J. Biochem. Eng. J. 64 (1996) 203–214.
[19] H. Wu, L. Zhuo, Q. He, X. Liao, B. Shi, Appl. Catal. A Gen. 366 (2009) 44–56.
[20] C. Jiang, V.V. Tsukruk, Adv. Mater. 18 (2006) 829–840.
[21] V.V. Tsukruk, V.N. Bliznyuk, D. Visser, A.L. Campbell, T.J. Bunning, W.W. Adams, Macromolecules 30 (1997) 6615–6625.
[22] G. Decher, J.D. Hong, Ber. Bunsenge. Phys. Chem. 95 (1991) 1430–1434.
[23] G. Decher, Science 277 (1997) 1232.
[24] D.M. Dotzauer, J. Dai, L. Sun, M.L. Bruening, Nano Lett. 6 (2006) 2268–2272.
[25] D.M. Dotzauer, A. Abusaloua, S. Miachon, J.-A. Dalmon, M.L. Bruening, Appl. Catal. B 91 (2009) 180–188.
[26] M. Liu, X. Zhu, R. Chen, Q. Liao, D. Ye, B. Zhang, J. Liu, G. Chen, K. Wang, Chem. Eng. J. 354 (2018) 35–41.
[27] P. Sonström, M. Bäumer, Phys. Chem. Chem. Phys. 13 (2011) 19270–19284.
[28] A.R. Tao, S. Habas, P. Yang, Small 4 (2008) 310–325.
[29] L. Ouyang, D.M. Dotzauer, S.R. Hogg, J. Macanás, J.-F. Lahitte, M.L. Bruening, Catal. Today 156 (2010) 100–106.
[30] T.C. Merkel, I. Pinnau, R. Prabhakar, B.D. Freeman, Gas and vapor transport properties of perfluoropolymers, in: Y. Yampolskii, I. Pinnau, B.D. Freeman (Eds.), Materials Science of Membranes for Gas and Vapor Separation, John Wiley & Sons, Chichester, 2006, pp. 251–270.
[31] I. Pinnau, L.G. Toy, J. Memb. Sci. 109 (1996) 125–133.
[32] M. Brzozowski, M. O'Brien, S.V. Ley, A. Polyzos, Acc. Chem. Res. 48 (2015) 349–362.
[33] M. O'Brien, N. Taylor, A. Polyzos, I.R. Baxendale, S.V. Ley, Chem. Sci. 2 (2011) 1250–1257.
[34] P. Koos, U. Gross, A. Polyzos, M. O'Brien, I. Baxendale, S.V. Ley, Org. Biomol. Chem. 9 (2011) 6903–6908.
[35] A. Polyzos, M. O'Brien, T.P. Petersen, I.R. Baxendale, S.V. Ley, Angew. Chem. Int. Ed. 50 (2011) 1190–1193.
[36] G. Wu, A. Constantinou, E. Cao, S. Kuhn, M. Morad, M. Sankar, D. Bethell, G.J. Hutchings, A. Gavriilidis, Ind. Eng. Chem. Res. 54 (2015) 4183–4189.
[37] B. Venezia, M. Douthwaite, G. Wu, M. Sankar, P. Ellis, G.J. Hutchings, A. Gavriilidis, Chem. Eng. J. 378 (2019) 122250.
[38] M. O'Brien, I.R. Baxendale, S.V. Ley, Org. Lett. 12 (2010) 1596–1598.
[39] H. Lee, S.M. Dellatore, W.M. Miller, P.B. Messersmith, Science 318 (2007) 426–430.
[40] J.H. Ryu, P.B. Messersmith, H. Lee, ACS Appl. Mater. Inerfaces 10 (2018) 7523–7540.
[41] J. Liebscher, R. Mrówczyński, H.A. Scheidt, C. Filip, N.D. Hădade, R. Turcu, A. Bende, S. Beck, Langmuir 29 (2013) 10539–10548.
[42] C. Huang, X. Wang, F. Yu, B. Yuan, C. Xie, S. Yu, Res. Chem. Intermed. 44 (2018) 13–26.
[43] Y. Piao, Y. Jang, M. Shokouhimehr, I.S. Lee, T. Hyeon, Small 3 (2007) 255–260.
[44] B. Lim, M. Jiang, P.H.C. Camargo, E.C. Cho, J. Tao, X. Lu, Y. Zhu, Y. Xia, Science 324 (2009) 1302–1305.
[45] B. Lim, M. Jiang, J. Tao, P.H.C. Camargo, Y. Zhu, Y. Xia, Adv. Funct. Mater. 19 (2009) 189–200.
[46] J. Liu, X. Zhu, Q. Liao, R. Chen, D. Ye, H. Feng, M. Liu, G. Chen, Chem. Eng. J. 332 (2018) 174–182.
[47] A. Corma, P. Concepción, P. Serna, Angew. Chem. Int. Ed. 46 (2007) 7266–7269.
[48] S. Kataoka, Y. Takeuchi, A. Harada, T. Takagi, Y. Takenaka, N. Fukaya, H. Yasuda, T. Ohmori, A. Endo, Appl. Catal. A Gen. 427-428 (2012) 119–124.
[49] E.A. Gelder, S.D. Jackson, C.M. Lok, Chem. Commun. (2005) 522–524.
[50] S. Mondini, A.M. Ferretti, A. Puglisi, A. Ponti, Nanoscale 4 (2012) 5356–5372.
[51] F.A. Harraz, S.E. El-Hout, H.M. Killa, I.A. Ibrahim, J. Catal. 286 (2012) 184–192.
[52] B.D. Adams, A. Chen, Mater. Today 14 (2011) 282–289.
[53] M. Guo, H. Li, Y. Ren, X. Ren, Q. Yang, C. Li, ACS Catal. 8 (2018) 6476–6485.
[54] G. Carturan, G. Facchin, G. Cocco, G. Navazio, G. Gubitosa, J. Catal. 82 (1983) 56–65.
[55] M. Liu, X. Zhu, R. Chen, Q. Liao, H. Feng, L. Li, Chem. Eng. J. 301 (2016) 35–41.